Pentacene Schottky diodes studied by impedance spectroscopy: Doping properties and trap response

Paul Pahner,[*] Hans Kleemann, Lorenzo Burtone, Max L. Tietze, Janine Fischer, Karl Leo,[†] and Björn Lüssem

Institut für Angewandte Photophysik, Technische Universität Dresden, George-Bähr-Strasse 1, 01069 Dresden, Germany

We study doping properties and charge carrier trap distributions in pentacene Schottky diodes doped by the fluorinated fullerene derivate $C_{60}F_{36}$ and 2,2'-(perdiylidene)dimalononitrile (F_6-TCNNQ) upon small signal excitation. We show that the charge carrier depletion zones present in these Schottky diodes are tunable by the applied bias and temperature. Mott-Schottky evaluations yield reduced doping efficiencies and dopant activation energies between 19 and 54 meV. In the low-frequency regime, we resolve additional capacitive contributions from inherent charge carrier traps. A Gaussian distributed trap center 0.6 eV above the hole transport level with a density in the range of 10^{16} cm^{-3} depending on the material purity is found to be an intrinsic feature of the pentacene matrix. Upon doping, the deep Gaussian trap center saturates in density and broad exponentially tailing trap distributions arise. Subsequent ultraviolet photoelectron spectroscopy measurements are conducted to inspect for energetic broadening due to doping.

I. INTRODUCTION

Molecular doping facilitated an enormous progress in the field of organic semiconductors and enabled a multitude of novel applications during the last decade. It has been demonstrated that the low conductivity, one of the main drawbacks of an intrinsic organic semiconductor, can be enhanced by several orders of magnitude when inserting a certain amount of electron- or hole-donating molecules.[1,2] Nowadays, doped transport layers play crucial roles in organic light emitting diodes (OLEDs)[3] or organic solar cells (OSCs)[4] where they ensure efficient charge carrier transport and form Ohmic contacts to corresponding electrodes. Moreover, promising device concepts such as alternating current driven OLEDs[5] or organic Zener diodes[6] require molecular doping for functionality.

In general, molecular $p(n)$-doping is considered as a two-step process: (i) ionization of the dopant accompanying electron transfer from the highest occupied molecular orbital (HOMO) of the host (dopant) molecule to the lowest unoccupied molecular orbital (LUMO) of the dopant (host) and (ii) dissociation of the strongly electrostatically bound charged couple generating a free charge carrier. Commonly, p-doping implies an electron affinity of the dopant EA at least equal or even larger than the ionization potential IP of the host for an efficient ionization (see Fig. 1). However, the dissociation of the charge transfer complex is not straightforward. Since the recombination of the charged couple is negligible at room temperature, the dissociation probability is governed by the electrostatic energetic disorder in close vicinity to the charges. Neighboring ionization centers distort the energetic landscape and it has been discussed controversially whether they effectively lower the Coulomb dissociation barrier,[7] form deep traps[8] or shape intermolecular hybridized states with the host material.[9]

However, it has been shown recently that even if ionization and breaking of the charged couple is perfect, the generation of free charge carriers at low doping concentrations is considerably hindered by inherent charge carrier traps.[10–15] Therefore a thorough understanding of the doping mechanism involves knowledge of the trap properties. As shown recently, energetically favorable trapping sites within the band gap originating from the pristine host material diminish the doping efficiency $\eta_p = p/N_A$ in p-doped N,N,N',N'-tetrakis(4-methoxyphenyl)-benzidine (MeO-TPD).[12,13] Upon increasing doping molecule concentrations, the Fermi level is pinned to the energy of the trap levels E_t, eventually moving towards the valence band edge after all trap states are filled. Only then, an increase in free charge carrier density p, mobility and doping efficiency is observable. A similar situation is reported for the n-doped buckminster fullerene C_{60}.[14–16]

Impedance spectroscopy can be used to study the doping process and the influence of charge carrier traps on doping. The presence of free charge carriers next to a metal surface induces the formation of a charge depletion zone to preserve equilibrium of the electrochemical potential within the semiconductor. Electric field and potential drop over this rectifying Schottky contact are obtained from the Poisson equation and widely known as level bending.[17] Under small-signal excitation, the capacitive response of the charge depletion zone can be used to study fundamental doping properties and provides access to the energetic trap distribution in the organic film. Recent publications proposed a model to describe the interaction of energetically distributed trap sites with the probe signal in organic solar cells, where energetically deep traps contribute to the capacitance spectra only in the lower-frequency range.[18–21]

In this paper, we systematically investigate the charge carrier depletion zone of pentacene (PEN) Schottky diodes doped with fluorinated fullerene derivate $C_{60}F_{36}$ as well as 2,2'-(perdiylidene)dimalononitrile (F_6-TCNNQ) by frequency-dependent impedance spectroscopy. Reducing the amount of incorporated dopant molecules to molar ratios (MR) below 0.01 ensures the formation of a controlled Schottky barrier with a charge carrier depletion zone in close vicinity to the metal contact, which is tunable by the applied bias and temperature. Mott-Schottky analyses yield reduced doping efficiencies, where free charge carriers are activated from shallow acceptor states. Analyzing the frequency-dependent capacitance response of the charge depletion zone and extending a recently reported trap occupancy model,[21] two prominent
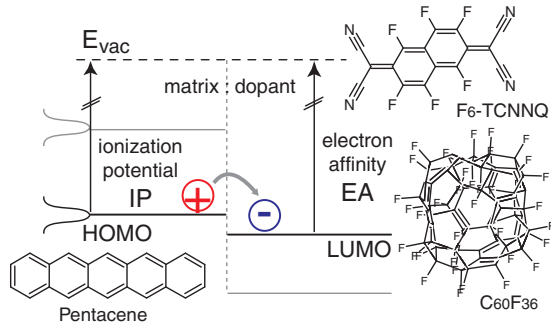
FIG. 1. (Color online) Energy level scheme for *p* doping in an organic matrix:dopant system. In our case, electrons are transferred from the HOMO state of a pentacene matrix molecule to the LUMO state of an adjacent $C_{60}F_{36}$ (F_6-TCNNQ) acceptor molecule, thus leaving a positively charged hole behind.

trap distributions are observable within the band gap, limiting the generation of free charge carriers. Both are characterized in spatial distribution, depth and density by comparing measured data and simulated capacitance spectra of the Schottky diodes. Ultraviolet photoelectron spectroscopy (UPS) and impedance spectroscopy studies on differently *p*-doped PEN are conducted to conclude on the origin of the found trap distributions.

II. EXPERIMENTAL

The organic Schottky junctions are prepared on cleaned glass substrates coated with a 90-nm-thick indium tin oxide (ITO) layer which acts as anode. A plasma treatment ensures a high electric work function and 1 nm of pure dopant $C_{60}F_{36}$ guarantees a reliable Ohmic contact. Consecutively, the organic layer and a 50 nm aluminum cathode are deposited by thermal vapor deposition at a base pressure of 10^{-7} to 10^{-8} mbar. The active device area is 6.35 mm². All samples are encapsulated with glass and UV-curable epoxy under nitrogen atmosphere directly after preparation. Schottky contact formation is achieved by co-evaporation of the host molecule pentacene (Sensient, Germany, 2x and 3x sublimated) as well as $C_{60}F_{36}$ (molar weight 1404.59 g/mol, Ionic Liquids Technologie GmbH, Germany)[22] or 2,2'-(perdiylidene)dimalononitrile (F_6-TCNNQ) (362.188 g/mol, Novaled AG, Germany) as dopants, respectively. If not stated explicitly, pentacene is used as 2x sublimated. Layer thickness and the amount of dopants are controlled via independent quartz crystal monitoring during evaporation. The doping concentration for the Schottky diodes is varied from 0.5 wt% (MR 0.0010 for $C_{60}F_{36}$ and MR 0.0039 for F_6-TCNNQ) down to 0.1wt % (MR 0.0002 for $C_{60}F_{36}$). The overall organic film thickness is 50 nm. Current-voltage measurements are performed with a Keithley 236 source measure unit. Impedance spectroscopy is carried out with an Autolab PGSTAT302N LCR Precision Meter in the range from 1 MHz down to 10 Hz. The amplitude of the oscillating signal is set to 15 mV to avoid nonlinear signal response. Upon small signal excitation, the out-of-phase current response is measured, directly displaying real (*R*) and imaginary part (*X*) of the impedance of the sample. All measurements are conducted in the dark while temperature-dependent measurements are performed in a continuous flow cryostat using liquid nitrogen where the

encapsulated sample remains in the vacuum. Electrical heating allows to keep the temperature stable in a region ±0.2 K around the set point.

The UPS experiments are performed on a Phoibos 100 system (SPECS Surface Nano Analysis GmbH, Germany) in a separate chamber directly attached to the evaporation chamber allowing sample transfer without breaking vacuum conditions. A sputter cleaned nonoriented silver foil covered with 4 nm of MeO-TPD as grow layer is used as UPS substrate. Details on measurement setup and procedure are described elsewhere.[12]

III. RESULTS AND DISCUSSION

A. Doping properties

As previously reported by Kleemann *et al.*, *p*-type doping by F_6-TCNNQ and the congeneric F_4-TCNQ molecule enhances the conductivity of pentacene thin films up to 0.1 S/cm.[23] Although such high values are desirable for commercial applications of organic electronics, only doping concentrations below a MR of 0.01 ensure the formation of a sufficiently large charge carrier depletion zone. For simplification of the analysis, all samples are asymmetric. Since the work function of ITO (4.7–4.9 eV)[24,25] is close to the HOMO of pentacene (5.0 eV),[26] and we employ contact doping, this contact is assumed to be Ohmic and its impact on the capacitance of the device is neglected.

As shown in Fig. 2 for PEN:$C_{60}F_{36}$, the Schottky diodes exhibit asymmetric *IV* characteristics. A pronounced plateau in phase angle $\varphi = \arctan R/X$ close to $-90°$ establishes for 0 V and moderate reverse voltages, which corresponds to a capacitive character of the devices. Subsequently, this frequency regime is used for capacitance voltage measurements enabling conclusions on the depletion capacitance of
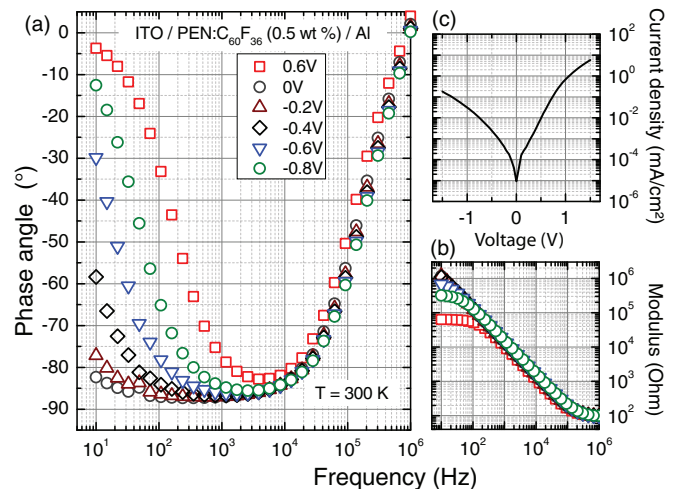

FIG. 2. (Color online) Impedance response of 50 nm PEN doped with 0.5 wt% $C_{60}F_{36}$ (MR 0.001) is shown, separated in phase angle φ (a) and modulus Z (b). Phase angles close to $-90°$ indicate an impedance governed by the (space charge depletion) capacitance of the device. For high frequencies, the modulus equals R_s of the device, while for very low frequencies, R_p dominates (compare Fig. 4). For $C(V)$ measurements, we choose a frequency in the stable-plateau regime around 5 kHz. The corresponding current-voltage characteristic emphasizes the diode behavior of the device (c).

the Schottky diodes. However, for frequencies above 10^4 Hz, the series resistance of the ITO starts to dominate the impedance response of the samples. The phase angle increases while the modulus $|Z| = \sqrt{R^2 + X^2}$ approaches the voltage independent value of the series resistance R_s (90–100 Ω). The increase in phase angle for frequencies $<10^2$ Hz is caused by the injection of charge carriers in forward direction (0.6 V) as well as an increasing contribution of leakage current for larger reverse bias. In physical terms, this is expressed by a parallel, voltage dependent leakage resistance R_p, resulting in a simplified R_s-$R_p C$ equivalent circuit model. Herein, the device capacitance C is calculated from[27]

$$C(\omega) = \frac{\Im[Y(\omega)]}{\omega} \tag{1}$$

using the imaginary part of the admittance Y and the small signal excitation frequency ω and corresponds to the thickness of the depletion zone of the Schottky diode. It is assumed, that the depleted layer exhibits no free charge carriers and behaves like a plate capacitor. Considering an abrupt junction and solving the Poisson equation, the charge carrier depletion zone width w_D next to the rectifying aluminum electrode ($W_f = 4.2$ eV) calculates as

$$w_D = \frac{\epsilon_0 \epsilon_r A}{C} = \sqrt{\frac{2\epsilon_0 \epsilon_r}{q N_A^-}(V_{\mathrm{bi}} - V)} \tag{2}$$

with $\epsilon_0 \epsilon_r$ as permittivity, A as sample area, V_{bi} as built-in voltage and N_A^- as density of ionized acceptor molecules.[17] Equation (2) can be easily transformed into the well-known Mott-Schottky relation

$$\frac{d}{dV}\frac{1}{C^2} = \frac{2}{q\epsilon_0\epsilon_r A^2}\frac{1}{N_A^-}. \tag{3}$$

The extent of the charge carrier depletion zone can be modulated as depicted in Fig. 3. By applying reverse bias, charge carriers are pushed even further away from the aluminum contact. The width of the depleted layer increases. Vice versa, the charge carrier depletion zone shrinks and finally collapses upon starting charge carrier injection for increasing forward bias. The slope of C^{-2} versus the applied voltage yields the density of ionized dopant molecules N_A^- within the junction. Herein, the dielectric constant $\epsilon_r = 5.8$ is taken separately from a series of measurements on fully depleted intrinsic pentacene diodes with various film thicknesses. In the doped samples, the generation of free charge carriers is temperature dependent, thus we observe a variation in the number of activated dopants from 9.9×10^{17} cm^{-3} (250 K) to 1.6×10^{18} cm^{-3} (310 K) for C$_{60}$F$_{36}$, and from 5.2×10^{18} cm^{-3} (213 K) to 7.1×10^{18} cm^{-3} (293 K) for F$_6$-TCNNQ. Calculating the ratio of ionized to introduced dopant molecules, we deduce a slightly larger doping efficiency for F$_6$-TCNNQ (64% at room temperature) compared to C$_{60}$F$_{36}$ (52%) (see inset Fig. 3). Considering N_A^- in the measured temperature range, we can deduce the activation energy ΔE_A of the doping process from

$$p = N_A^- \propto \exp\left(-\frac{\Delta E_A}{k_B T}\right) \tag{4}$$

with p denoting the charge carrier density of free holes, T the sample temperature and k_B as Boltzmann constant.
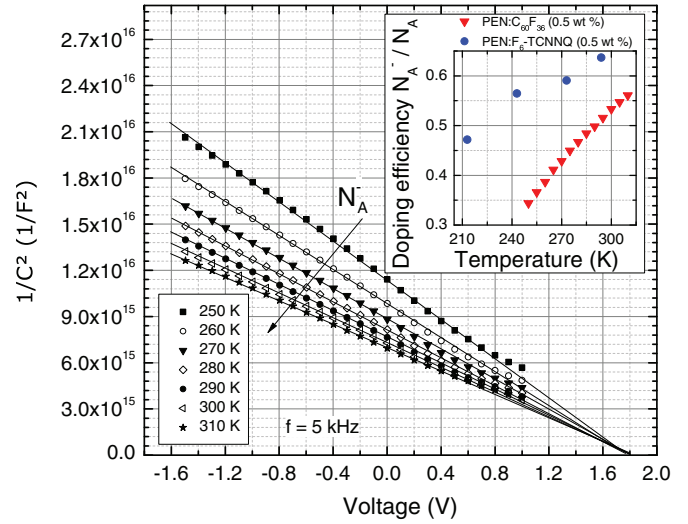

FIG. 3. (Color online) Mott-Schottky plot deduced from capacitance-voltage measurements at a frequency of 5 kHz, shown here for 0.5 wt% C$_{60}$F$_{36}$-doped pentacene and temperatures from 250 K up to 310 K. The slope of the plots reveals the number of ionized acceptor molecules N_A^-, which is decreasing for lower temperatures. Equally, the computed doping efficiency drops (see inset), whereby a constant amount N_A of dopants introduced in the organic layer is assumed.

Figure 4(c) shows the results for both dopants in the pentacene matrix. For C$_{60}$F$_{36}$, we obtain an activation energy of 54 meV (625.8 K), whereas significantly less activation energy is required for F$_6$-TCNNQ (19 meV, 219.4 K). For comparison, prior results yield an activation energy of 16 meV in 0.5 wt% C$_{60}$F$_{36}$-doped MeO-TPD.[12] Although the energy values can
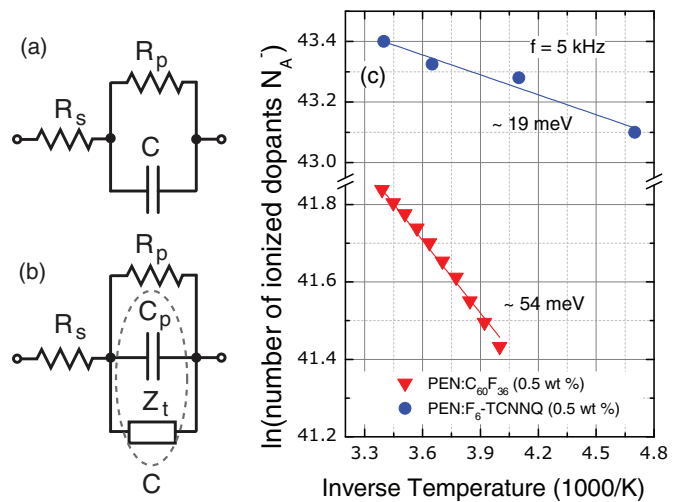

FIG. 4. (Color online) (Left) Applied equivalent circuit models for interpretation of the obtained capacitance spectra. Approaching measurement frequencies $>10^3$ Hz, a simplified model with only series (R_s) and parallel resistance (R_p) as well as sample capacitance C is sufficient (a). For the interpretation of the low frequency response we use a recently reported additional trap distribution element (Z_t)[21] (b). (Right) Arrhenius plots reveal the activation energy of shallow acceptor states introduced by dopant molecules C$_{60}$F$_{36}$ and F$_6$-TCNNQ in the pentacene matrix (c).

be attributed to a doping activation from shallow acceptor sites, the physical interpretation of these numbers is not straightforward.

Since the HOMO energies of the molecules in organic semiconductors are broadened due to disorder and polarization by neighboring molecules—a fact which is more pronounced for less crystaline materials[28]—the effective density of states is commonly described with one or more Gaussian distribution functions. As both, matrix and dopant molecules, exhibit this feature, the assumption of a distinct activation energy ΔE_A is rather problematic. However, incorporating only low doping, it has been shown that the introduction of a discrete effective transport level E_V,

$$E_V = E_0 + \frac{\sigma^2}{2k_B T}, \qquad (5)$$

holds.[10] Although the transport level depends on the broadening of the HOMO energies, it is independent from the charge carrier concentration for concentrations in the range of 10% to 1% of the site density or less. For such a situation, the Fermi level is far away from the center of the density of states (DOS) and the application of Boltzmann statistics is valid. Nevertheless, the nature of ΔE_A can only be understood in statistical terms. As the widths of Gaussian DOS of organic semiconductors are typically in the range of 0.2 eV and E_V and the predicted acceptor level E_A are separated by a few 100 meV only,[12] it is hard to link the activation energy directly to the EA of the dopant and the IP of pentacene. Both dopants exhibit similar electron affinities ($C_{60}F_{36}$: 5.38 eV, F_6-TCNNQ: 5.37 eV)[22,29] sufficiently larger than the reported value for the IP of pentacene (5.0 eV).[26] Therefore, their differences in activation energy and doping efficiency can not entirely explained in terms of different dopant-to-host charge transfer probabilities. Instead, the differences might point towards a more complex interaction of dopant, host and inherent trap distributions which determines the generation as well as the activation of free charge carriers[13,30] and is studied in detail in the following.

B. Trap response

Using Eq. (1), the frequency-dependent capacitance functions of pentacene doped with $C_{60}F_{36}$ and F_6-TCNNQ are shown in Fig. 5. In the first-order approximation, an equivalent circuit as depicted in Fig. 4(a) and introduced above is sufficient to explain at least the swing of the obtained capacitance functions between 5×10^3 and 10^6 Hz (dotted lines in Fig. 5). The usage of an equivalent circuit fitting routine (done with the commercial program ZVIEW®) helps to acquire data on series and parallel resistance as well as the capacitance of the charge depletion layer. However, an additional capacitance contribution is observed for lower frequencies (compare Fig. 5), visible as an increasing offset for decreasing frequencies. This indicates the presence of trap states.

Recent publications reported on the interaction of distributed charge carrier traps with the applied probe signal in impedance spectroscopy. As known from early literature on inorganic Schottky junctions, inherent trapping sites are able to populate and depopulate within a specific time frame
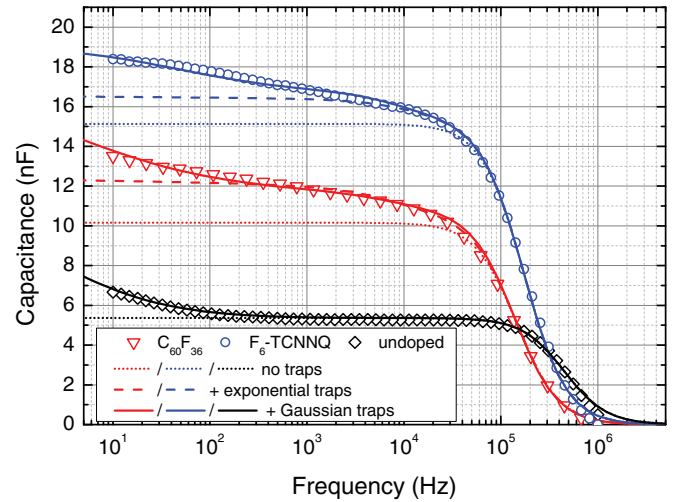

FIG. 5. (Color online) Capacitance spectra for pentacene Schottky diodes, comprising dopant molecules $C_{60}F_{36}$ (red) or F_6-TCNNQ (blue) (0.5 wt%) at zero bias. The measured data (symbols) are compared with the simulated capacitance spectra: only calculating the impact of the depletion layer (dotted line), incorporating exponentially distributed trap states (dashed line), and featuring additional deeper lying Gaussian distributed trap states (solid line). For comparison, an entirely undoped pentacene sample is plotted (black), exhibiting a similar deep trap but no exponential trap distribution (black solid line).

depending on their energetic depth thus altering the capacitive response of the device.[31] Extending this idea as previously developed for organic solar cells,[18,20,21] the device can be described by a combination of equivalent circuit model and statistical Boltzmann approach [see Fig. 4(b)]. Hereby, charge carriers are stored in trap sites in the bulk and influence the electric field within the charge depletion layer. Assuming a generic trap distribution $g(E)$ and its interaction with one distinct transport level E_V, the additional trap capacitance function can be calculated by[18]

$$Y_t(\omega) = Z_t^{-1}(\omega)$$
$$= j\omega \frac{q^2}{k_B T} \int_{E_V}^{E_C} \frac{g(E) f_t(E) [1 - f_t(E)]}{1 + j\omega/\omega_t} dE. \quad (6)$$

Hereby, the trap occupation with holes p_t is given by

$$p_t = \int g(E) [1 - f_t(E)] dE \qquad (7)$$

with $f_t(E)$ being the Fermi-Dirac function. Typically, the trap distribution function $g(E)$ is represented by a Gaussian density of trap states $g'(E)$ with

$$g'(E) = \frac{N_{t,g}}{\sqrt{2\pi\sigma^2}} \exp\left[-\frac{(E - E_{t,g})^2}{2\sigma^2}\right] \qquad (8)$$

with a defined energetic depth $E_{t,g}$ referring to the transport level and the center of the Gaussian trap DOS, a broadening factor σ and a trap concentration $N_{t,g}$. Moreover, we include the possibility of exponentially decaying traps $g''(E)$ with

$$g''(E) = \frac{N_{t,\exp}}{k_B T_0} \exp\left(-\frac{E_V - E}{k_B T_0}\right) \qquad (9)$$

above the transport level towards the middle of the band gap with the concentration $N_{t,\exp}$ and the scaling factor T_0. Upon small signal excitation, the traps respond with the characteristic trap frequency

$$\omega_t = \frac{\varepsilon}{f_t} \qquad (10)$$

with the time constant for the release of traps

$$\varepsilon(E_t) = \beta N_V \exp\left(\frac{E_V - E_t}{k_B T}\right). \qquad (11)$$

The recombination rate β is computed from

$$\beta = \frac{e(\mu_h + \mu_e)}{\varepsilon_0 \varepsilon_r} \qquad (12)$$

according to Langevin recombination theory for disordered organic semiconductors.[32] With values of $\mu_h \approx 10^{-2}$ cm^2/Vs and $\mu_e \approx 10^{-3}$ cm^2/Vs (measured separately inhouse) we obtain $\beta \approx 10^{-9}$ cm^3/s, which is one order of magnitude higher than in previous findings.[18,21,33] We note, that a deviation of β of one order of magnitude leads to an error of approximate 50 meV in trap depth. To receive the entire trap capacitance contribution, the integral Eq. (6) is solved, i.e., the Fermi level over the whole device is computed. This is done by performing one-dimensional drift diffusion simulations for the layer structure, following the previously reported approach of Schober *et al.*[34] Utilizing the Scharfetter-Gummel discretization scheme[35] and the extended Gaussian disorder model,[36,37] the Schottky diodes are considered as single carrier devices with one Ohmic and one thermionic injection contact. The energy levels of the contacts ($E_{F,\text{ITO}} = 4.8$ eV, $E_{F,\text{Al}} = 4.2$ eV) and the pentacene matrix ($EA = 3.2$ eV, $IP = 5.1$ eV) are measured separately inhouse by ultraviolet photoelectron spectroscopy. The doping concentrations determining the level bending are chosen in accordance to the values obtained from the Mott-Schottky evaluations of the previous section. At first, the energy level diagrams are computed without any inherent trap distributions. After an estimation of the trap properties utilizing the introduced model, the energy level diagrams are redefined using the obtained data and cross checked once more.

As C$_{60}$F$_{36}$ and F$_6$-TCNNQ have a large difference in molar weight, more F$_6$-TCNNQ than C$_{60}$F$_{36}$ dopant molecules are introduced at a fixed weight ratio of dopant and host. Thus, even considering the same doping efficiency of both materials in the pentacene host, F$_6$-TCNNQ forms a narrower charge carrier depletion zone, i.e., a larger capacitance plateau (compare Fig. 5). This fact coincides with the less extended energy level bending obtained from simulation for F$_6$-TCNNQ (23 nm) compared to C$_{60}$F$_{36}$ (33 nm) (see Fig. 6). Without assuming traps, measured and simulated capacitance functions of C$_{60}$F$_{36}$ as well as F$_6$-TCNNQ doped pentacene samples deviate strongly for frequencies below 10^4 Hz. By introducing exponentially distributed traps ($N_{t,\exp} = 4.5 \times 10^{16}$ cm^{-3}, $k_B T_0 = 319$ meV for PEN:C$_{60}$F$_{36}$ and $N_{t,\exp} = 6.2 \times 10^{16}$ cm^{-3}, $k_B T_0 = 302$ meV for PEN:F$_6$-TCNNQ) the simulated capacitance functions agree well with the measured data for frequencies above 10^2 Hz. Below this frequency, a second contribution is emerging, which we can describe as a deep, relatively narrow ($\sigma = 0.055$ eV) Gaussian shaped trap distribution ($N_{t,g} = 1.2 \times 10^{17}$ cm^{-3}, $E_{t,g} = 0.60$ eV for
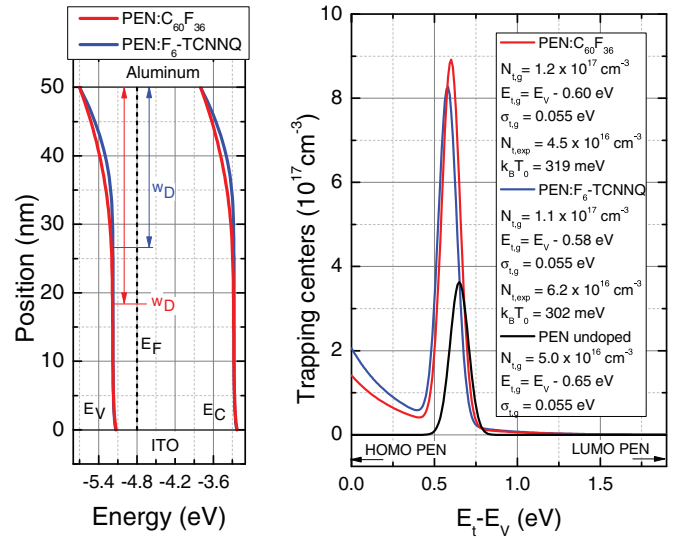

FIG. 6. (Color online) (Left) Energy level diagram for measured Schotty diodes obtained by drift-diffusion simulation. Energy levels are chosen in accordance to known UPS data, dopant concentrations as measured in previous part. Due to higher molar ratio of F$_6$-TCNNQ in the pentacene bulk, we exhibit a smaller depletion zone w_D (23 nm), compared to C$_{60}$F$_{36}$ doped pentacene (32 nm). (Right) For modeling the measured capacitance spectra, we include a combination of exponentially tailing and deeper lying Gaussian distributed trap centers. In samples of undoped pentacene, only a deeper lying trap is visible.

PEN:C$_{60}$F$_{36}$ and $N_{t,g} = 1.1 \times 10^{17}$ cm^{-3}, $E_{t,g} = 0.58$ eV for PEN:F$_6$-TCNNQ). All computed trap densities are displayed in Fig. 6 (right).

Obviously, both additional trap contributions present in the doped films are energetically rather independent of the actual species of the incorporated dopant molecule. From this data, it is not clear if the found trap distributions can be attributed to the (pristine) matrix material itself or originate from the doping process. While deeper lying Gaussian traps are commonly caused by material impurities or structural defects, exponential distributions are mostly affiliated to tail states of the density of states of the semiconductor. Therefore we examine completely undoped pentacene (2x sublimated) devices, comprising the same contact structure. None of them feature shallow trap states which we described by an exponential distribution in the doped devices in the previous section. Representatively, the measured capacitance spectra for a 50 nm intrinsic pentacene device is shown in Fig. 5 as well (black symbols). Down to a frequency of approximately 500 Hz, a pronounced and very stable capacitance plateau is visible, matching the geometric capacitance of the sample and thus indicating an entirely depleted semiconductor. Very shallow traps which were modelled by introducing an exponential distribution in the doped samples, are not visible and do not alter the simulated spectrum. However, the rise in the capacitance spectra below 500 Hz is very similar to those in PEN:C$_{60}$F$_{36}$ and PEN:F$_6$-TCNNQ. Again, this is successfully described by a Gaussian trap DOS ($N_{t,g} = 5.0 \times 10^{16}$ cm^{-3}, $E_{t,g} = 0.65$ eV, and $\sigma = 0.055$ eV).

C. Interaction between doping and traps

Comparing the found trap distributions, it is most likely that the deeper lying Gaussian distributed traps (0.58–0.65 eV) are characteristic for the pentacene host, since they occur in doped as well as undoped samples independently. However, the introduction of dopant molecules increases the *observable* amount of deep traps. Additionally, exponentially tailing trap states become visible. This tendency could hint for either (i) an increased energetic disorder in the films, which would be in accordance to predictions made by Arkhipov *et al.* who stated that Coulomb interactions between ionized dopant centers and generated free charge carriers increase the DOS tailing and cause the formation of additional deep traps,[38] or (ii) a sequential filling of existing trap states due to Fermi level

shift upon doping. Regarding Eq. (6), only occupied trap states contribute to the trap impedance and are visible in impedance spectroscopy.

Following these considerations, we conduct UPS, measurements on PEN:$C_{60}F_{36}$ films (undoped, MR 0.002, 0.02, 0.33) to examine the shape of the HOMO DOS and check for structural broadening upon doping. The results are depicted in Fig. 7. The UPS data is resolved in arbitrary units, normalized to its peak maximum and a constant noise level is fitted. Initially broadened due to disorder and polarization, the DOS needs to be described by a combination of two Gaussian distributions ($E_{0,1} = -1.93$ eV, $E_{0,2} = -1.66$ eV), while the latter is chosen to describe the high-energy slope of the HOMO. Additional tailing states towards the center of the band gap have to be included and are fitted with an exponential distribution relative to the center of the combined Gaussian E_0. For low doping ratios (MR 0.002), the tailing properties ($N_\beta = 0.027, k_B T_0 = 0.346$ eV) remain nearly constant compared to undoped pentacene ($N_\beta = 0.021, k_B T_0 = 0.356$ eV).

It has to be noted that we can not directly assign exponential tailing states found by UPS to the populated trap states observed by impedance spectroscopy. Since charge carrier transport in organic semiconductors is described by hopping transport over localized states, it is hard to distinguish between barely mobile and already trapping states by inspecting the shape of the DOS in regions close to the resolution limit of UPS without further assumptions on position and strictness of the charge carrier transport level. However, regarding only the manifestation of the DOS, no substantial additional energetic broadening is visible at doping concentrations (MR 0.002 and below) relevant for our devices. Only for a strongly increased amount of incorporated dopants, the combined Gaussian as well as the exponential tailing ($k_B T_0 = 0.399$ eV
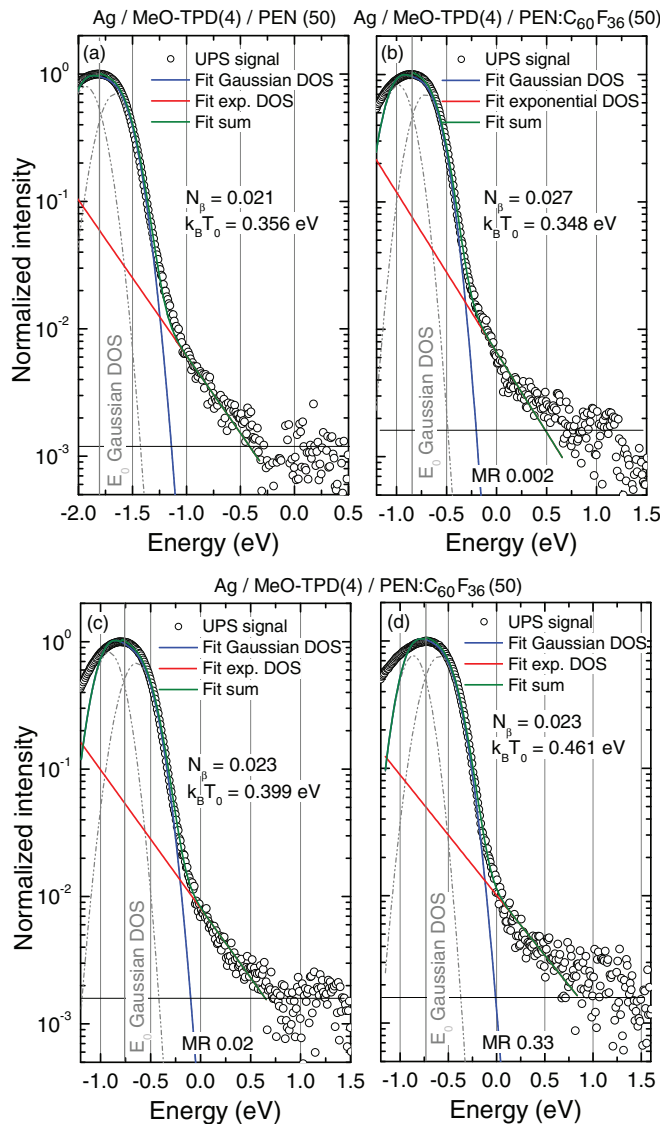

FIG. 7. (Color online) UPS spectra of (a) undoped and (b)–(d) $C_{60}F_{36}$-doped pentacene films (MR 0.002, 0.02, 0.33). The HOMO DOS is fitted using a combined Gaussian (blue) and an exponential distribution (red). Hereby, exponential tail states are visible even for the intrinsic host, while tailing increases upon moderate (MR 0.02) to high (MR 0.33) doping. All values (arbitrary units) are normalized to the peak value and a constant noise level is fitted (black line).
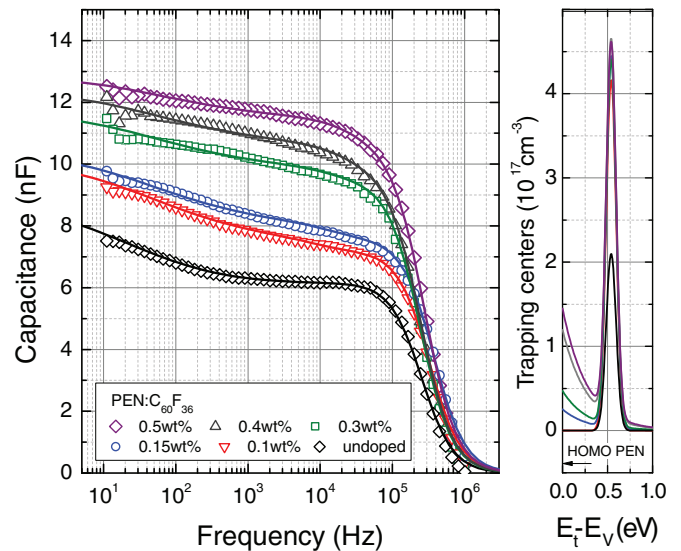

FIG. 8. (Color online) (Left) Measured capacitance spectra for $C_{60}F_{36}$-doped pentacene (3x sublimated) films with various doping concentrations (0 V, $T = 295$ K) (symbols) and respective simulated capacitance spectra (lines). (Right) With increasing doping concentration thus shifting the Fermi level towards the HOMO edge, the deeper Gaussian distributed traps are saturated ($N_t \approx 6 \times 10^{16}$ cm^{-3}) and exponentially distributed traps are strongly pronounced.

TABLE I. Number of ionized dopants N_A^- and measured trap densities $N_T^+ = N_{t,g} + N_{t,\mathrm{exp}}$ for different doping concentrations N_A in ITO/PEN:$C_{60}F_{36}$/Al -Schottky diodes. Doping efficiencies are given as N_A^-/N_A.

wt%	N_A (cm^{-3})	N_A^- (cm^{-3})	$N_{t,g}$ (cm^{-3})	$N_{t,\mathrm{exp}}$ (cm^{-3})	N_T^+ (cm^{-3})	N_A^-/N_A
undoped	. . .	. . .	2.9×10^{16}	0	2.9×10^{16}	. . .
0.10	5.7×10^{17}	5.6×10^{17}	5.8×10^{16}	0	5.8×10^{16}	0.98
0.15	8.6×10^{17}	6.6×10^{17}	6.1×10^{16}	7.0×10^{15}	6.8×10^{16}	0.77
0.30	1.7×10^{18}	1.1×10^{18}	6.0×10^{16}	1.3×10^{16}	7.3×10^{16}	0.65
0.40	2.3×10^{18}	1.2×10^{18}	6.2×10^{16}	3.3×10^{16}	9.5×10^{16}	0.52
0.50	2.9×10^{18}	1.3×10^{18}	6.1×10^{16}	4.0×10^{16}	1.0×10^{17}	0.45

for MR 0.02 and $k_B T_0 = 0.461$ eV for MR 0.33) in the UPS spectra are significantly additionally broadened [see Figs. 7(c) and 7(d)]. These findings point towards former results on crystalline materials that change their morphology with strongly increased doping ratios eventually resulting in very lowly conducting, nearly amorphous films for high concentrations.[23]

Utilizing different doping concentrations [0.5 wt% (MR 0.0010) to 0.1 wt% (MR 0.0002)] of $C_{60}F_{36}$ in our pentacene Schottky diodes however, points strongly towards sequential trap filling as governing mechanism for the rise in measured trap density in Fig. 6. As depicted in Fig. 8, starting from a value of $N_{t,g} = 2.9 \times 10^{16}$ cm^{-3} for the undoped device, the deep Gaussian distributed trap ($E_{t,g} = 0.6$ eV, $\sigma = 0.055$ eV) saturates at around $N_{t,g} = 6 \times 10^{16}$ cm^{-3} for doped devices. While we do not see a contribution of exponential trap states to the capacitance spectrum for 0.1 wt%, the number of observed exponential trap states $N_{t,\mathrm{exp}}$ ($k_B T_0 = 0.275$ eV) is gradually increasing for a transition from 0.15 to 0.5 wt%. Details on the extracted trap distributions are given in Table I. Energetic depth and width of the trap distributions are kept constant for reasons of comparability and agree very well with the prior results.

Presumably due to improved material quality (3x sublimated in contrast to 2x sublimated pentacene for the previous measurements), the overall amount of deep Gaussian traps is reduced in this measurement series. Nevertheless, we observe a sequential population of traps by shifting the Fermi-Level towards the HOMO level, which is in good agreement with our presented model. The major trap contribution is expected to originate from regions of the device having the Fermi level crossing the trap distribution thus enabling to respond to the excitation signal. The overall doping efficiency N_A^-/N_A drops from around 100% to 45%. This trend could hint for either a shift of the Fermi level below the acceptor level of the dopant (*impurity reserve*)[12] or an increasing aggregation of dopant molecules, but encourages further investigations. In conclusion, our results show that the increase in measured trap density is not caused by inducing additional defect states upon doping. Instead, the increasing trap response in impedance spectroscopy is due to a proceeding population of traps due to a shift of the Fermi level to the HOMO edge by doping.

IV. CONCLUSION

Besides numerous advanced experimental techniques,[39–42] impedance spectroscopy provides access to energetic trap distributions in organic films and allows to study fundamental doping properties at the same time. In this paper, we systematically investigate the capacitive response of p-doped pentacene Schottky diodes. Changing bias voltage and junction temperature, we modulate the space charge depletion layers which allows to conclude on doping efficiency and activation energy of the doping process in the pentacene matrix. Examining the low-frequency regime of the obtained capacitance spectra of the Schottky junctions, we propose a method to disclose inherent trapping site distributions of organic semiconductors. Involving knowledge on the energy level diagram, which has to be gained from drift diffusion simulations, we are able to resolve exponential trap distributions decaying from the HOMO edge towards the band gap and deeper lying Gaussian distributed trap centers in the organic semiconductor. For undoped pentacene, we observe a Gaussian distributed trap center ($E_t - E_V \approx 0.6$ eV) as an inherent feature of the host material. Its density is dependent on the number of sublimation steps of the pentacene and decreases by a factor of 2 from two to three steps. Besides, exponential tail states exist even in the intrinsic sample, but they are not filled and thus cannot respond on any excitation. Upon low doping, the Fermi level starts to shift towards the HOMO egde and trap states are subsequentially populated. At first, the deep Gaussian states saturate at 6×10^{16} cm^{-3} (3x sublimated). In the following, an increasing number of exponential tail states becomes visibile ($\approx 10^{16}$ cm^{-3}). Additional substantial energetic broadening due to the disturbance of the crystal lattice upon doping is examined by UPS but not observed for doping concentrations up to MR 0.002.

*paul.pahner@iapp.de
†karl.leo@iapp.de

[1]B. Maennig, M. Pfeiffer, A. Nollau, X. Zhou, K. Leo, and P. Simon, Phys. Rev. B **64**, 195208 (2001).

[2]J. Blochwitz, M. Pfeiffer, T. Fritz, and K. Leo, Appl. Phys. Lett. **73**, 729 (1998).

[3]S. Reineke, F. Lindner, G. Schwartz, N. Seidler, K. Walzer, B. Lüssem, and K. Leo, Nature (London) **459**, 234 (2009).

[4]R. Fitzner, E. Reinhold, A. Mishra, E. Mena-Osteritz, H. Ziehlke, C. Körner, K. Leo, M. Riede, M. Weil, O. Tsaryova, A. Weiß, C. Uhrich, M. Pfeiffer, and P. Bäuerle, Adv. Funct. Mater. **21**, 897 (2011).

[5]M. Fröbel, A. Perumal, T. Schwab, M. C. Gather, B. Lüssem, and K. Leo, Org. Electron. **14**, 809 (2013).

[6]H. Kleemann, R. Gutierrez, F. Lindner, S. Avdoshenko, P. D. Manrique, B. Lüssem, G. Cuniberti, and K. Leo, Nano Lett. **10**, 4929 (2010).

[7]A. Mityashin, Y. Oliver, T. van Regemorter, C. Rolin, S. Verlaak, N. G. Martinelli, D. Beljonne, J. Cornil, J. Genoe, and P. Heremans, Adv. Mater. **24**, 1535 (2012).

[8]J.-H. Lee, D.-S. Leem, and J.-J. Kim, Org. Electron. **11**, 486 (2010).

[9]I. Salzmann, G. Heimel, S. Duhm, M. Oehzelt, P. Pingel, B. M. George, A. Schnegg, K. Lips, R.-P. Blum, A. Vollmer, and N. Koch, Phys. Rev. Lett. **108**, 035502 (2012).

[10]V. I. Arkhipov, P. Heremans, E. V. Emelianova, G. J. Adriaenssens, and H. Bässler, Appl. Phys. Lett. **82**, 3245 (2003).

[11]Y. Zhang, B. de Boer, and P. W. M. Blom, Phys. Rev. B **81**, 085201 (2010).

[12]M. L. Tietze, L. Burtone, M. Riede, B. Lüssem, and K. Leo, Phys. Rev. B **86**, 035320 (2012).

[13]M. L. Tietze, K. Leo, and B. Lüssem, Org. Electron. **14**, 2348 (2013).

[14]S. Olthof, S. Mehraeen, S. K. Mohapatra, S. Barlow, V. Coropceanu, J.-L. Bredas, S. R. Marder, and A. Kahn, Phys. Rev. Lett. **109**, 176601 (2012).

[15]S. Olthof, S. Singh, S. K. Mohapatra, S. Barlow, S. R. Marder, B. Kippelen, and A. Kahn, Appl. Phys. Lett. **101**, 253303 (2012).

[16]T. Menke, D. Ray, J. Meiss, K. Leo, and M. Riede, Appl. Phys. Lett. **100**, 093304 (2012).

[17]S. M. Sze and K. K. Ng, *Physics of Semiconductor Devices* (Wiley, New York, 1981).

[18]J. Bisquert, Phys. Rev. B **77**, 235203 (2008).

[19]J. M. Montero and J. Bisquert, J. Appl. Phys. **110**, 043705 (2011).

[20]L. Burtone, D. Ray, K. Leo, and M. Riede, J. Appl. Phys. **111**, 064503 (2012).

[21]L. Burtone, J. Fischer, K. Leo, and M. Riede, Phys. Rev. B **87**, 045432 (2013).

[22]R. Meerheim, S. Olthof, M. Hermenau, S. Scholz, A. Petrich, N. Tessler, O. Solomeshch, B. Lüssem, M. Riede, and K. Leo, J. Appl. Phys. **109**, 103102 (2011).

[23]H. Kleemann, C. Schünemann, A. A. Zakhidov, M. Riede, B. Lüssem, and K. Leo, Org. Electron. **13**, 58 (2012).

[24]J. Blochwitz, T. Fritz, M. Pfeiffer, K. Leo, D. M. Alloway, P. A. Lee, and N. R. Armstrong, Org. Electron. **2**, 97 (2001).

[25]R. Schlaf, H. Murata, and Z. H. Kafafi, J. Electron Spectrosc. Relat. Phenom. **120**, 149 (2001).

[26]W.-K. Kim, K. Hong, and J.-L. Lee, Appl. Phys. Lett. **89**, 142117 (2006).

[27]E. Barsoukov and J. R. Macdonald, *Impedance Spectroscopy: Theory, Experiment, and Applications* (Wiley, New York, 2005).

[28]H. Bässler, Phys. Status Solidi B **175**, 15 (1993).

[29]P. K. Koech, A. B. Padmaperuma, L. Wang, J. S. Swensen, E. Polikarpov, J. T. Darsell, J. E. Rainbolt, and D. J. Gaspar, Chem. Mater. **22**, 3926 (2010).

[30]H. Kleemann, K. Leo, and B. Lüssem, J. Appl. Phys. **111**, 123722 (2012).

[31]Y. Hasegawa and Y. Abe, Phys. Status Solidi A **70**, 615 (1982).

[32]J. J. M. van der Holst, F. W. A. van Oost, R. Coehoorn, and P. A. Bobbert, Phys. Rev. B **80**, 235202 (2009).

[33]M. Schmeits and N. D. Nguyen, Phys. Status Solidi A **202**, 2764 (2005).

[34]M. Schober, M. Anderson, M. Thomschke, J. Widmer, M. Furno, R. Scholz, B. Lüssem, and K. Leo, Phys. Rev. B **84**, 165326 (2011).

[35]D. Scharfetter and H. Gummel, IEEE Trans. Electron Devices **16**, 64 (1969).

[36]W. F. Pasveer, J. Cottaar, C. Tanase, R. Coehoorn, P. A. Bobbert, P. W. M. Blom, D. M. deLeeuw, and M. A. J. Michels, Phys. Rev. Lett. **94**, 206601 (2005).

[37]R. Coehoorn and S. L. M. van Mensfoort, Phys. Rev. B **80**, 085302 (2009).

[38]V. I. Arkhipov, P. Heremans, E. V. Emelianova, and H. Bässler, Phys. Rev. B **71**, 045214 (2005).

[39]D. V. Lang, J. Appl. Phys. **45**, 3023 (1974).

[40]S. Neugebauer, J. Rauh, C. Deibel, and V. Dyakonov, Appl. Phys. Lett. **100**, 263304 (2012).

[41]N. von Malm, R. Schmechel, and H. von Seggern, Synth. Met. **126**, 87 (2002).

[42]J. Schafferhans, A. Baumann, C. Deibel, and V. Dyakonov, Appl. Phys. Lett. **93**, 093303 (2008).